




Inhalation of Silver Silicate Nanoparticles Leads to Transient and Differential Microglial Activation in the Rodent Olfactory Bulb

Toxicologic Pathology
2022, Vol. 50(6) 763–775
© The Author(s) 2022
Article reuse guidelines:
sagepub.com/journals-permissions
DOI: 10.1177/01926233221107607
journals.sagepub.com/home/tpx


Huong Huynh^{1,2*} , Priya Upadhyay^{2*}, Cora H. Lopez², Malia K. Miyashiro², Laura S. Van Winkle^{2,3}, Sara M. Thomasy^{4,5}, and Kent E. Pinkerton^{2,3} 

Abstract

Engineered silver nanoparticles (AgNPs), including silver silicate nanoparticles (Ag-SiO₂ NPs), are used in a wide variety of medical and consumer applications. Inhaled AgNPs have been found to translocate to the olfactory bulb (OB) after inhalation and intranasal instillation. However, the biological effects of Ag-SiO₂ NPs and their potential nose-to-brain transport have not been evaluated. The present study assessed whether inhaled Ag-SiO₂ NPs can elicit microglial activation in the OB. Adult Sprague-Dawley rats inhaled aerosolized Ag-SiO₂ NPs at a concentration of 1 mg/ml for 6 hours. On day 0, 1, 7, and 21 post-exposure, rats were necropsied and OB were harvested. Immunohistochemistry on OB tissues were performed with anti-ionized calcium-binding adapter molecule 1 and heme oxygenase-1 as markers of microglial activation and oxidative stress, respectively. Aerosol characterization indicated Ag-SiO₂ NPs were sufficiently aerosolized with moderate agglomeration and high-efficiency deposition in the nasal cavity and olfactory epithelium. Findings suggested that acute inhalation of Ag-SiO₂ NPs elicited transient and differential microglial activation in the OB without significant microglial recruitment or oxidative stress. The delayed and differential pattern of microglial activation in the OB implied that inhaled Ag-SiO₂ may have translocated to the central nervous system via intra-neuronal pathways.

Keywords

engineered nanomaterials, neurotoxicity, inhalation, immunohistochemistry, olfactory bulb, microglia, rodent study

Introduction

Silver nanoparticles (AgNPs), including silver silicate nanoparticles (Ag-SiO₂ NPs), are engineered transition-metal nanomaterials with diverse commercial applications. AgNPs are one of the most widely used metallic nanoparticles due to their broad-antimicrobial properties.¹ AgNPs are used in wound dressings and as protective coatings for medical supplies.^{2,3} AgNPs are also used in various consumer products, from cosmetics to food storage containers.⁴ Exposure to AgNPs can occur through dermal and ocular absorption, oral ingestion, or inhalation.^{5–9} Inhalation of AgNPs may occur during manufacturing or usage of aerosolized commercial products or drug therapies containing silver, such as over-the-counter nasal spray treatments for respiratory infections. AgNPs are manufactured in various forms, with different compositions, sizes, shapes, and surface coatings, all of which confer unique physical and chemical properties.^{10–12} Silver silicate (Ag-SiO₂) is a type of AgNPs supported on silica, which reduces particle agglomeration.¹³ Ag-SiO₂ NPs are also used as antimicrobial additives for wound dressings and in catalytic reduction of toxic dyes in industries.^{14–16}

Inhaled AgNPs can become entrapped in the fluid lining layer over the olfactory mucosa before reaching the olfactory

epithelium.¹⁷ From there, several possible pathways to the central nervous system (CNS) have been suggested. These include the (1) intra-neuronal pathway via uptake into olfactory nerve and trigeminal nerve, with retrograde axonal transport through neurons to the brain; (2) extra-neuronal pathway via transcellular transport across the sustentacular cells and paracellular transport across the tight junctions between sustentacular cells

¹ William R Pritchard Veterinary Medical Teaching Hospital, University of California, Davis, Davis, California, USA

² Center for Health and the Environment, University of California, Davis, Davis, California, USA

³ Department of Anatomy, Physiology & Cell Biology, School of Veterinary Medicine, University of California, Davis, Davis, California, USA

⁴ Department of Surgical and Radiological Sciences, School of Veterinary Medicine, University of California, Davis, Davis, California, USA

⁵ Department of Ophthalmology and Vision Science, School of Medicine, University of California, Davis, Davis, California, USA

*Huong Huynh and Priya Upadhyay contributed equally to this research.

Corresponding Author:

Kent E. Pinkerton, Center for Health and the Environment, University of California, Davis, One Shields Ave., Davis, CA 95616, USA.

Email: kepinkerton@ucdavis.edu

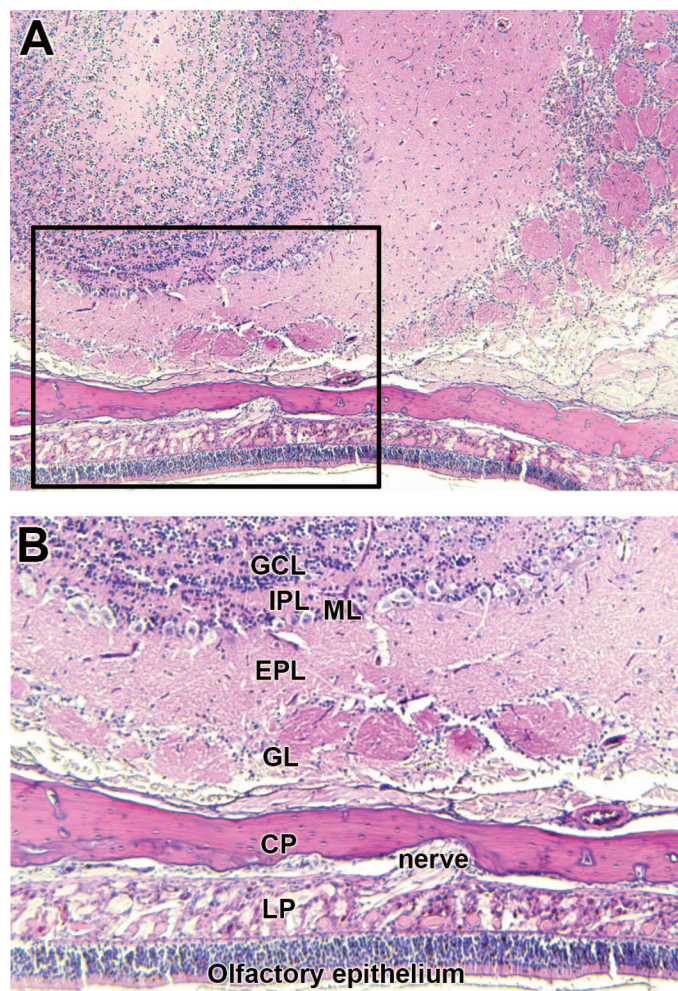


Figure 1. Representative brightfield microscopy images of 5- μ m thick, hematoxylin and eosin-stained tissue sections of rat nasal tissue and olfactory bulb (OB). Panel A shows a transverse section of the OB at original objective 5X. Box identifies a section of the OB shown in panel B at original objective 10X. Panel B shows the lamellar structure composed of histologically distinct layers of the OB. CP indicates cribriform plate; EPL, external plexiform layer; GCL, granular cell layer; GL, glomerular layer; IPL, internal plexiform layer; LP, lamina propria; ML, mitral cell layer.

and olfactory sensory neurons; (3) systemic pathway through translocation across the rich vasculature of the respiratory epithelium, absorption into lymphatics, ingestion following clearance of NPs via the mucociliary escalator with subsequent gastrointestinal absorption into the hepatic portal circulation.¹⁸⁻²⁰ Intra-neuronal nose-to-brain translocation via the olfactory nerve pathway is also utilized by viruses such as herpesvirus, influenza A virus, and SAR-CoV-2 virus, which are similarly sized to AgNPs, to gain access to the CNS.^{21,22}

AgNPs have been found in the olfactory bulb (OB) following inhalation of AgNPs.^{23-26(p1873)} Previous studies suggested that NPs can reach the OB via the olfactory pathway, similar to how odorant information is relayed to the CNS.²⁶⁻²⁸ The OB receives odorant molecules from the olfactory epithelium in the

nasal cavity via the olfactory sensory nerve fascicles.^{29(p1)} The OB has a lamellar structure with several histologically distinct layers (Figure 1).³⁰ These layers, in the order of most superficial to deep, include the glomerular layer (GL), external plexiform layer (EPL), mitral cell layer (MCL), internal plexiform layer (IPL), and granule cell layer (GCL). Odorant molecules from the nasal cavity arrive at the GL of the OB before information is relayed to cells of the deeper layers of the OB and finally the primary olfactory cortex.^{29(p2)}

Microglia are resident macrophages of the CNS and are beneficial in immune surveillance, synaptic plasticity, neuronal repair, and neurogenesis.³¹⁻³⁴ However, prolonged and/or excessive microglial activation following inhalation of NPs can be detrimental due to associated upregulation of toll-like receptors and release of pro-inflammatory cytokines and chemokines.³⁵⁻³⁷ Inhaled AgNPs may be sufficiently immunogenic to elicit an in vivo pro-inflammatory response in the OB via microglial activation.^{26(p1874)} The cytotoxicity of AgNPs is thought to be primarily due to the release of ionic silver (Ag^+) into the biological environment.³⁸⁻⁴⁰

The primary objectives of the present study were to determine whether acutely inhaled Ag-SiO₂ NPs activate resting microglia in the OB, and if there is differential activation of microglia in different histological layers of the OB. Rats were exposed to aerosols of Ag-SiO₂, and their OB were harvested immediately after exposure on day 0 (D0) and on post-exposure day 1, 7, and 21 (D1, D7, D21, respectively). Ten-micrometer-thick OB sections were immunostained for anti-ionized calcium-binding adapter molecule 1 (anti-Iba1) to identify the site and morphology of microglia in the OB and with heme oxygenase-1 (HO-1) as a marker of oxidative stress in the OB.

Materials and Methods

Powdered Ag-SiO₂ NPs

The Ag-SiO₂ NPs used in the present study were synthesized, characterized, and supplied in powder form by the National Institute of Environmental Health Sciences Centers for Nanotechnology Health Implications Research Consortium. Ag-SiO₂ NPs were synthesized by flame spray pyrolysis as silver (~8 nm) supported on silica (~7 nm) (3.79% w/w).^{41,42} The powdered Ag-SiO₂ NPs were on average 10.64 nm \pm 7.10 nm in diameter before suspension in endotoxin-free water to a 1 mg/ml concentration for aerosolization. The primary particle size, primary particle size distribution, and size factor were characterized by transmission electron microscope (TEM) image analysis. Crystallinity, density, and chemical composition were characterized by x-ray diffraction, pycnometer, and inductively coupled plasma mass spectrometry (ICP-MS), respectively.

Animal Care

Adult, 12-week-old male Sprague-Dawley rats were obtained from Envigo laboratory (Fremont, CA). Upon arrival, the rats

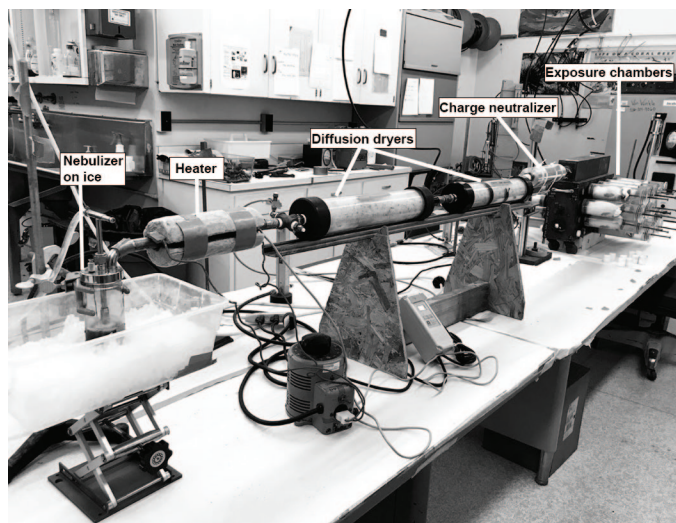


Figure 2. Aerosolization and exposure system.

were randomly assigned to two exposure groups, Ag-SiO₂ ($n = 4$ per time point) or filtered air ($n = 8$; pooled from D1 and D21 post-exposure). The rats were housed two per cage in filter-top polycarbonate cages in an animal facility with high-efficiency particulate air filters, maintained in a 12-hour dark/light cycle under standard temperature and given ad libitum access to a standard laboratory rodent diet (Purina 5001, Newco Distributors, Rancho Cucamonga, CA) and water. Rats were allowed to acclimate for at least 1 week prior to the experimental exposure. During the acclimation period, the rats were conditioned to remain in the inhalation exposure tubes (Teague Enterprises, Woodland, CA) for progressively longer periods. The conditioning exercises were performed to minimize confinement stress during the experimental exposure. Animals were handled following guidelines from the National Institutes of Health and Institutional Animal Care and Use Committee of the University of California, Davis.

Aerosolization of Ag-SiO₂ NPs

Rats were exposed to either filtered room air or Ag-SiO₂ aerosol generated by the aerosol nebulization system located at the Center for Health and the Environment, University of California, Davis (Figure 2). The Ag-SiO₂ suspension was sonicated (QSonica Sonicators; 500 W, 20kHz, 90% Amp), kept on ice to reduce particle aggregation, and aerosolized with a BGI 6-jet Collision nebulizer (Waltham, MA) into fine droplets. Air for the nebulizer was compressed with an oil-free compressor (California Air Tools, San Diego, CA), dehumidified with compressed air dryers (Wilkerton, Richland, MI), and filtered with a Motor Gard M-610 filter (Motor Gard, Manteca, CA). The fine nebulized droplets passed through a custom-fabricated heater and two diffusion dryers (TSI, Shoreview, MN) to remove any remaining water. The resulting dried particles then passed through a Krypton-85 charge-neutralizer to reduce static and

minimize particle agglomeration before entering the 48-port nose-only exposure system connected by steel piping.⁴³

Nose-Only Inhalation Exposure

Rats were placed into the nose-only exposure tubes, one rat per tube, for a single, 6-hour exposure to either filtered air or aerosolized Ag-SiO₂. Rats were monitored for their presence and activity while in the inhalation chamber for the entire duration of the exposure period. The average temperature and humidity in the exposure room was 56°F and 54%, respectively.

Characterization of the Aerosolized Ag-SiO₂ NPs

Air samples were collected throughout the 6-hour exposure period, and aerosol characterization was performed using a protocol previously described.⁴⁴ Briefly, the mass concentration and particle size distribution of the aerosolized Ag-SiO₂ NPs were determined via gravimetry and an eight-stage Mercer-style cascade impactor, respectively, using samples collected onto 25-mm diameter Pallflex membrane filters (catalog number 28150-925, Pall Life Sciences, Port Washington, NY). The silver mass was determined by x-ray fluorescence (XRF; Chester Labnet, Tigard, OR) with samples collected on 25-mm diameter Pall Teflo filters (catalog number 28139-131, Pall Life Sciences); and the average particle diameter was measured using aerosolized particles collected onto formvar carbon film (carbon grids 200 mesh, catalog number FCF200-Cu, Electron Microscopy Sciences, Hatfields, PA) and examined via a Phillips CM-12 transmission electron microscope operating at 120kV.

Tissue Collection and Preparation

Ag-SiO₂ NPs-exposed rats were euthanized on D0 (immediately after the exposure), D1, D7, and D21 post-exposure with an intraperitoneal injection of Beuthanasia-D at 7.5 ml/kg (MWI Veterinary Supply Company, Los Angeles, CA 90074). Control animals were necropsied on D1 and D21 after the exposure. Cardiac puncture was performed, and blood was collected in a 12-ml round bottom tube for centrifugation at 2000 revolutions per minute (rpm) for 15 minutes. The resulting blood plasma was collected and stored at -80°C for later use. Following blood collection, the trachea was cannulated, and the left main bronchus was clamped. The right middle, caudal, and accessory lobes were lavaged, flash-frozen, and stored at -80°C for later use. Briefly, the lobes were lavaged three times with a single 7-ml aliquot of sterile phosphate-buffered saline (PBS, Sigma Aldrich, St Louis, MO) in a 12-ml syringe for collection of bronchoalveolar lavage fluid (BALF). The BALF was collected in a 15-ml round bottom tube and centrifuged for 15 minutes at 2000 rpm and 4°C. The resulting BALF supernatant was decanted and stored for further analysis, while the cell pellet was resuspended in 2 ml of sterile PBS. Trypan blue was used to count the total viable and non-viable cells. A 100-μl aliquot

of resuspended cells was used to prepare cytospin slides for cell differentials. The left lung was unclamped and inflation-fixed at a hydrostatic pressure of 30 cm with 4% paraformaldehyde for 1 hour. The fixed lung was subsequently stored in 4% paraformaldehyde for 24 hours before transfer to 70% ethanol. A separate manuscript is being prepared to evaluate the potential pulmonary toxicity following inhalation of Ag-SiO₂ NPs.

The heads were decapitated, brains were removed, and the remaining head was fixed in 4% paraformaldehyde for 24 hours and stored in 70% ethanol. The heads and nasal cavities were decalcified along with the OB using 0.5-M ethylenediaminetetraacetic acid (EDTA, pH = 8; Thermo Fisher Scientific, Waltham, MA) at room temperature for 2 weeks. A total of four transverse sections of nasal cavity per rat were obtained following a standard protocol.⁴⁵ Then, one sagittal section of the decalcified heads was obtained per rat. Sagittal tissue orientation was chosen so that the nasal cavity and OB tissues are on the same slide for silver detection in the nose and the OB with autometallography. All tissues were embedded in Paraplast (Fisher Scientific, Swedesboro, NJ), cut with a microtome to 5- μ m and 10- μ m thick sections and put onto slides (catalog number 12-550015, Fisherbrand, Thermo Fisher Scientific, Waltham, MA).

Immunohistochemistry

For each rat, three slides of OB were immunostained for anti-Iba1, and one slide of OB was immunostained for HO-1 to visualize microglia and assess for oxidative stress, respectively. The OB sections were deparaffinized in three changes of toluene for 5 minutes each and rehydrated in 100%, 95%, and 70% ethanol for 2 minutes each before immersion in EDTA (Thermo Fisher Scientific, pH = 8) at 123°C for 2 minutes, and 85°C for 10 seconds. The sections were then cooled for 45 minutes and washed for 5 minutes under gentle running tap water. Endogenous peroxidase was blocked with 3% hydrogen peroxide for 10 minutes, followed by a quick dip in distilled water and three washes in phosphate-buffered saline with 1000 μ l Tween 20 (PBST; Sigma Aldrich) at 2 minutes each. Nonspecific proteins were blocked with Protein Block (catalog number X0909; Dako, Carpinteria, CA) for 20 minutes at room temperature. The sections incubated with anti-Iba1 (ab 153696, Abcam Inc, Cambridge, MA), at a 1:1000 dilution with PBST, were incubated overnight at room temperature. The sections incubated with HO-1 (ab 13243, Abcam Inc), at a 1:700 dilution with PBST, were incubated for 1 hour at room temperature. Negative-control tissue sections were not incubated with the primary antibody. Sections were then washed in PBST following a protocol of two washes of brief 20 dips followed by two washes at 5 minutes each. The sections were then incubated with the secondary antibody, horseradish peroxidase-labeled polymer for rabbit (catalog number K4403; Dako), for 30 minutes at room temperature and washed twice in PBST with occasional agitation for 5 minutes each. Each section was incubated with 100 μ l of 3,3'-Diaminobenzidine (DAB) and substrate (catalog number K3468; Dako) for 5 minutes at room temperature. DAB solution was tipped off each section onto lab

paper. Sections were washed briefly in distilled water twice and counterstained with Harris Hematoxylin (MasterTech, Inc, Lodi, CA) and coverslipped with ClearMount permanent mounting medium (Thermo Fisher Scientific). Immunohistochemistry staining was evaluated qualitatively.

Microglial Visualization and Characterization

The OB sections immunostained for Iba1 were divided into four histologically distinct layers for photomicrography. These layers consisted of the olfactory nerve layer (ONL), glomerular layer (GL), external plexiform layer (EPL), and inner layers (IL). Each IL consisted of the mitral cell layer, internal plexiform layer, and granule cell layer, grouped as one layer because these layers were difficult to distinguish from each other at original objective 20X. Microglial abundance and morphology were evaluated in three randomly sampled non-overlapping fields per histologically distinct layer for a total of twelve fields per histological section, one section per animal, four animals in each Ag-SiO₂ post-exposure group and eight animals in sham control at original objective 20X on a Zeiss AxioLab.A1 microscope. All microglia were manually counted in each of the twelve randomly captured, non-overlapping fields to determine microglial abundance, and microglial morphology was evaluated to determine resting and activation states. The ratio of activated to resting microglia was calculated for sham control and each of the five exposure groups. The protocol was repeated for each of the four histologically distinct layers (ONL, GL, EPL, and IL) in the OB sections. Four investigators evaluated microglial abundance and morphology in a blinded fashion, and their scores were averaged.

Microglial morphology was categorized as resting or activated as a mean of evaluating the OB response to inhalation of Ag-SiO₂ and as an indirect assessment of NP translocation to the CNS. Microglial morphology is associated with different microglial phenotypes.^{46,47} Resting microglia surveils for changes in the microenvironment and has a small cell body with extensively ramified processes. The processes are highly motile, undergoing continuous cycles of de novo formation and disappearance without a net change in the total number of processes to dynamically scan the environment without disturbing pre-existing neuronal structures.^{48,49} Once microglia sense changes in the microenvironment such as the presence of pro-inflammatory stimuli such as lipopolysaccharide and interferon gamma or cytokines such as interleukin 4 and interleukin 10, they change their morphology into an amoeboid form with enlarged cell bodies and retracted, thickened processes to mediate phagocytic activity, suppress inflammation, or mediate tissue remodeling.⁵⁰ This study classified microglia as resting or activated based on previously accepted criteria.^{26,27,51} Resting microglia were defined as cells with at least two highly ramified processes extending at least twice the length of a small nucleus. Activated microglia were defined as cells with significantly shortened ramified processes extending from a slightly enlarged cell nucleus.

Oxidative Stress

The OB sections immunostained for HO-1 were treated in similar fashion as sections immunostained for Iba1. HO-1 expression was evaluated qualitatively, as present or not present, in twelve randomly sampled non-overlapping fields per histologically distinct layers per histological section, one section per animal, four animals in each Ag-SiO₂ post-exposure group and eight animals in sham control at original objective 20X on a Zeiss AxioLab.A1 microscope.

Statistical Analysis

Data were analyzed with Jamovi 1.6 statistical software (Sydney, Australia). No animals were excluded from statistical analysis. Shapiro-Wilk and Levene's tests were performed to confirm normality and homoscedasticity, respectively.⁵² Statistically significant differences in microglial abundance and microglial activation were determined by Welch's one-way analyses of variance (ANOVAs).⁵³ Games-Howell post hoc tests were used to identify significant differences between specific groups. These tests were performed at a significance level of $P < .05$. Data are presented as group means \pm standard error.

Results

Ag-SiO₂ Aerosol Characterization

Aerosol characterization suggested that the Ag-SiO₂ NPs in nanopure water were sufficiently aerosolized with moderate agglomeration. The mean Ag-SiO₂ aerosol mass concentration measured by gravimetry was 4.9 ± 2.3 mg/m³, and the Ag concentration measured by XRF was 0.17 ± 0.01 mg/m³. These results suggested that suspension of Ag-SiO₂ NPs in nanopure water did not alter the mass concentration of the aerosol. The median aerosol diameter measured by cascade impactor was 1.9 ± 0.3 μ m, and the size (diameter) distribution of the Ag-SiO₂ NPs based on TEM ranged from 21 to 370 nm (Figures 3 and 4). The aerosol diameter measured by the cascade impactor suggested that there was particle agglomeration, but size distribution based on TEM suggested that approximately 50% of Ag-SiO₂ NPs were less than 100 nm in diameter and small enough to be deposited in the nasal epithelium.⁵⁴

Transient and Differential Microglial Activation in the OB Without Microglial Recruitment

Microglial morphology in the OB was categorized as resting or activated (Figure 5). Microglial numbers were counted to determine microglial abundance in the OB (Figure 6, panel A) and in each histologically distinct layer of the OB in sham control and Ag-SiO₂ post-exposure groups (Figure 6, panels B, C, D, and E). The ratio for activated to resting microglia were calculated for the entire OB (Figure 7, panel A) and for each histologically distinct layer of the OB (Figure 7, panels

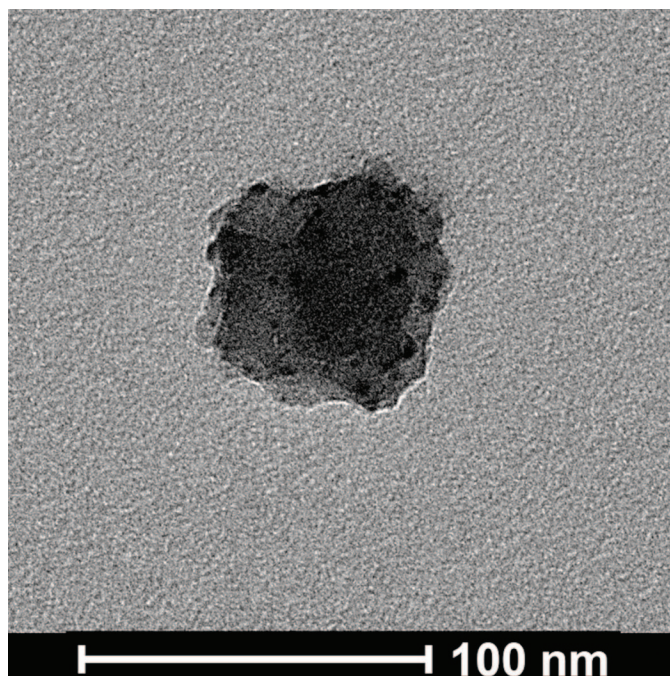


Figure 3. Transmission electron microscopy image at original objective 120kX of a silver silicate (Ag-SiO₂) nanoparticle obtained during a single, 6-hour aerosolization period.

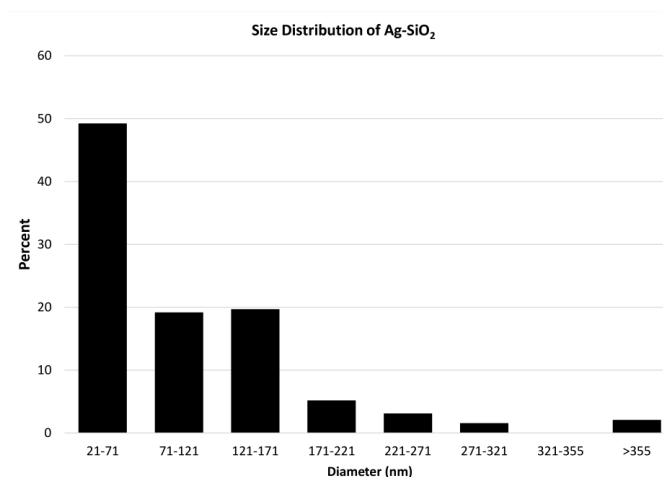


Figure 4. Graph of the size (diameter) distribution of aerosolized silver silicate (Ag-SiO₂) nanoparticles measured by transmission electron microscopy.

B, C, D, and E) in sham control and Ag-SiO₂. After Ag-SiO₂ versus filtered air exposure, there was significant ($P = .02$) microglial activation in the OB, compared with sham control, with elevated ratios of activated to resting microglia noted on D1 and D7 post-exposure and a return to control concentration by D21 (Figure 7, panel A). In the ONL, there was a notable but non-significant ($P = .08$) increase in the ratio of activated to resting microglia on D1 and D7 compared with sham control (Figure 7, panel B). In contrast, the

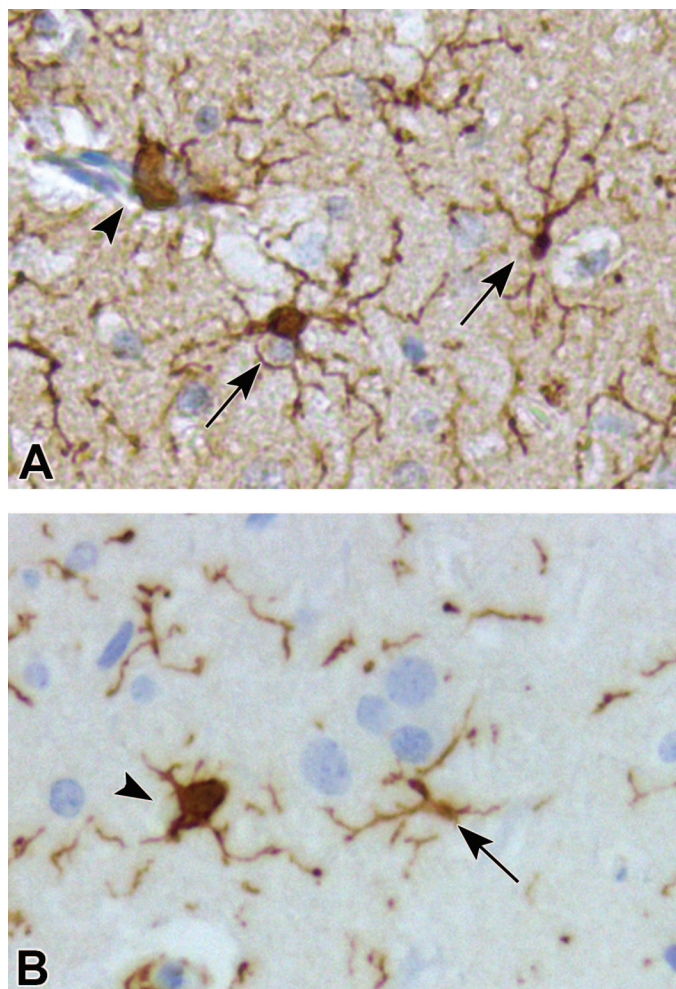


Figure 5. Representative brightfield microscopy images of olfactory bulb tissue sections, at original objective 20X, with anti-ionized calcium-binding adapter molecule 1 (anti-Iba1; panel A) and anti-heme oxygenase-1 (anti-HO-1; panel B) immunohistochemical stains. Resting microglia are indicated by arrows and characterized by a small cell body with ramified processes. Activated microglia are indicated by arrowheads and characterized by a large cell body with retracted processes.

GL of the OB in exposed rats demonstrated a significant increase ($P = .01$) compared with sham control in the proportion of activated to resting microglia on post-exposure D1 [Figure 7, panel C, and Figure 8]. In the EPL and IL, there were no notable inter-group differences in the ratio of activated to resting microglia (Figure 7, panels D and E). There was no significant difference in microglial abundance between sham control versus exposed group at any time point post-exposure, which suggested a lack of microglial recruitment (Figure 6).

Mild Oxidative Stress in the OB

Sparse HO-1 immunoreactivity was noted in the ONL on D0 and the EPL on D1 and D7 (Figure 9). Negative and sham controls showed no immunoreactivity.

Discussion

The primary objectives of the present study were to determine whether acute inhalation of Ag-SiO₂ NPs induced microglial activation and, and if so, whether microglial activation differed between the distinct histologic layers of the OB. Based on our results, we concluded that an acute (single, 6-hour) inhalation exposure to Ag-SiO₂ NPs elicited slightly delayed and transient microglial activation on D1 and D7 post-exposure, particularly in the GL, without significant microglial recruitment to the OB. There was also evidence of mild oxidative stress in the OB at D0, D1, and D7 post-exposure. The temporal and differential pattern of microglial activation in the OB implied that inhaled Ag-SiO₂ NPs are immunogenic in the biologic environment and may have translocated to the CNS via intra-neuronal and systemic pathways to induce a mild pro-inflammatory response.

In this study, the aerosolized silver concentration averaged 0.17 ± 0.01 mg/m³. The Occupational Safety and Health Administration (OSHA)⁵⁵ set the exposure limit for silver at 0.01 mg/m³ per 8-hour time weighted average. Maximal time weighted average of aerosolized silver concentration of up to 0.289 mg/m³ has been detected in silver manufacturing plants.⁵⁶ Our study's aerosolized silver concentration can be correlated to an environment with high occupational exposure to aerosolized silver without personal safety measures.

A trend was observed for an increased ratio of activated-to-resting microglia in groups exposed to Ag-SiO₂ NPs compared with filtered air controls, with the highest elevation noted on D1 and D7 post-exposure, which returned to control concentration by D21 (Figure 7, panel A). These observations suggested a transient pro-inflammatory response in the OB to inhaled Ag-SiO₂ NPs. The inflammatory response mediated by microglia can help directly sequester NPs for digestion. Microglial cells may recognize NPs through surface toll-like receptors (TLR2 and TLR4) and can internalize NPs via phagocytosis, micropinocytosis, and clathrin-mediated endocytosis.^{36,37,57,58} Microglia may also be activated to remodel damaged neuronal tissues, as AgNPs and Ag⁺ have been shown to induce apoptosis mediated by reactive oxygen species and phagocytosis mediated by tissue necrosis factor- α and interleukin-1 β .^{38,59-61}

Activation of microglia in the OB implied that inhaled Ag-SiO₂ NPs may have translocated to the CNS to induce a pro-inflammatory response. However, it is unclear from the present study which route NPs take to enter the CNS. Delayed microglial activation on D1 and D7 post-exposure without significant activation on D0 is suggestive of intra-neuronal pathway as a possible route for inhaled Ag-SiO₂ NPs to arrive at the OB. This presumption is supported by previous studies, which demonstrated that particles traveling from the olfactory epithelium to the OB take minutes to make this journey via extra-neuronal pathways, 18 to 36 minutes via fast axonal transport (a type of intra-neuronal transport), and approximately 5 days with slow axonal transport (another type of intra-neuronal transport).^{20,27}

Systemic pathway is another possible route for Ag-SiO₂ NPs to enter the CNS. A kinetic time course study showed that

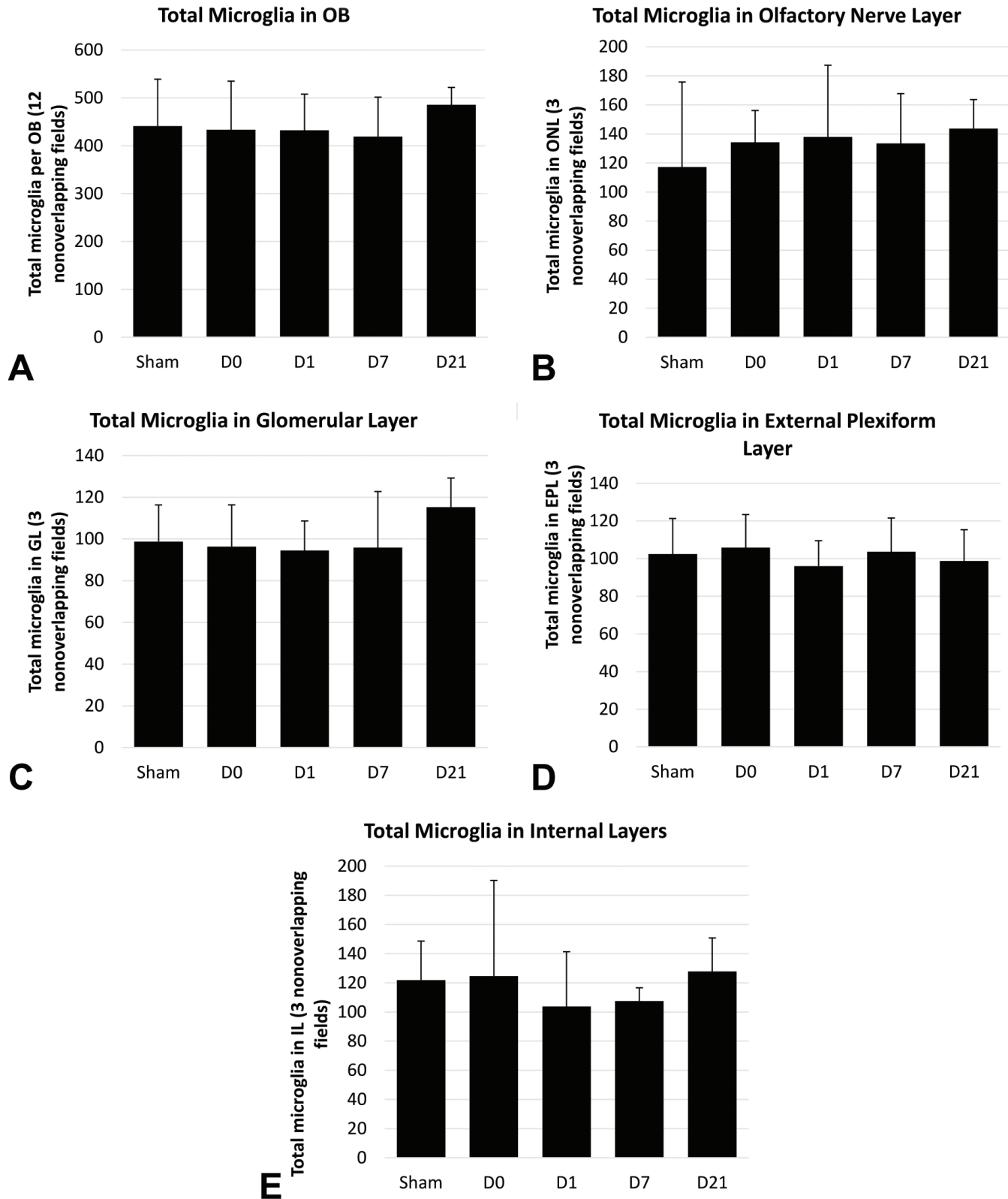


Figure 6. Total (panel A) and differential (panels B-E) microglial cell counts in the olfactory bulb (OB). Microglial cells were counted in twelve non-overlapping fields per animal. Differential microglial cell counts were determined using three non-overlapping fields per histologically distinct layer per olfactory bulb per animal. The analysis was done at original objective 20X, and four animals in each Ag-SiO₂ post-exposure group and eight animals in sham control were examined. Welch's one-way ANOVAs and post hoc Games-Howell tests were used to compare groups exposed to filtered air (control) or aerosolized silver silicate nanoparticles and euthanized 0, 7, 14, or 21 days post-exposure (D0, D7, D14, and D21, respectively). Each value shown in the graphs is a group mean \pm standard error.

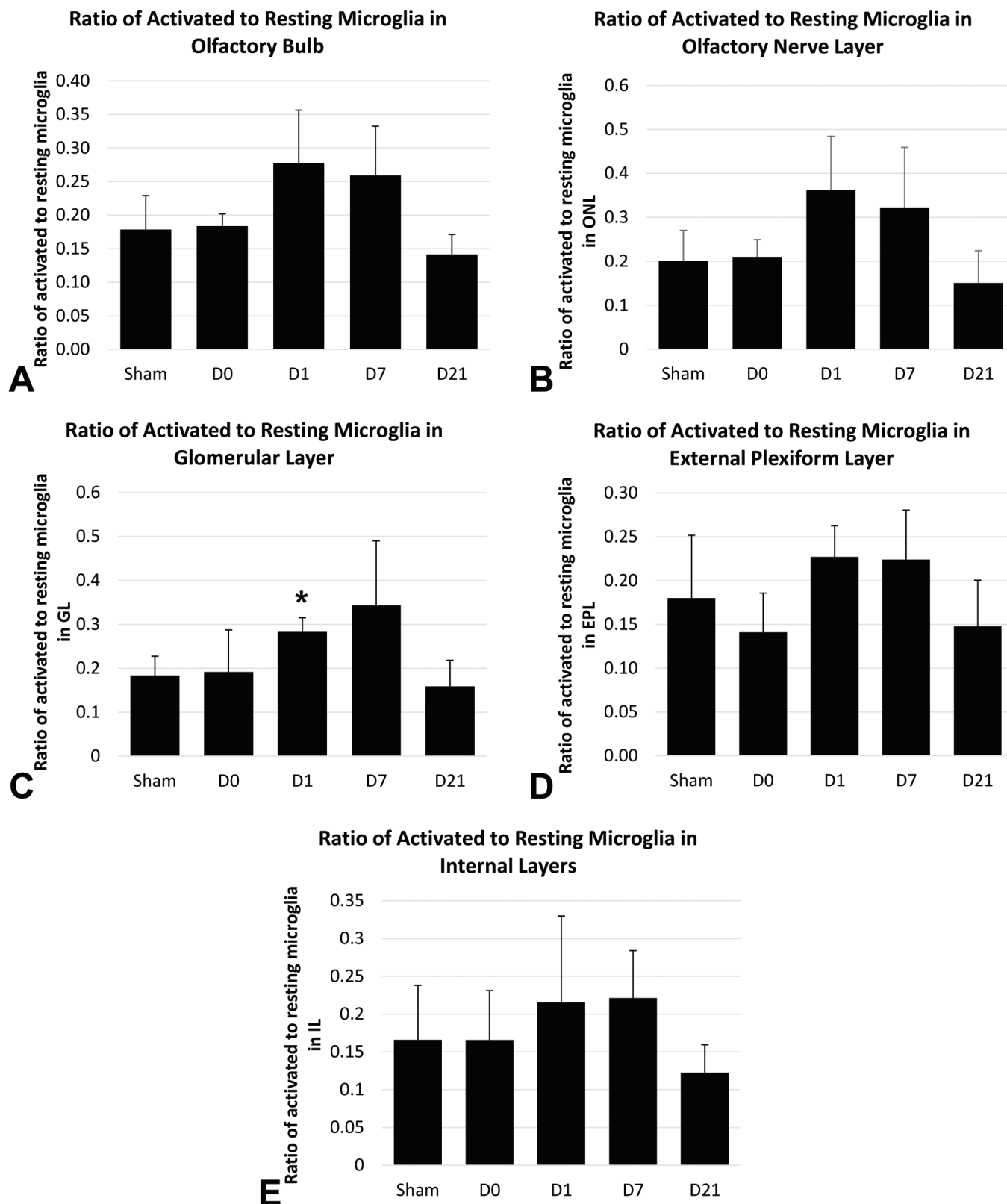


Figure 7. Inter-group comparisons of the ratio of activated to resting microglia in the olfactory bulb (panel A) and histologically distinct layers of the olfactory bulb (panels B-E). Microglia were morphometrically evaluated in twelve non-overlapping fields per olfactory bulb (OB) per animal, with three fields per histologically distinct layer. The analysis was done at original objective 20X, and four animals in each Ag-SiO₂ post-exposure group and eight animals in sham control were examined. Welch's one-way ANOVAs and post hoc Games-Howell tests were used to compare groups exposed to filtered air (sham control) or aerosolized silver silicate nanoparticles and euthanized 0, 7, 14, or 21 days post-exposure (D0, D7, D14, and D21, respectively). Each value shown in the graphs is a group mean \pm standard error. The asterisk (*) represents a significant ($P = .01$) difference from the sham control group.

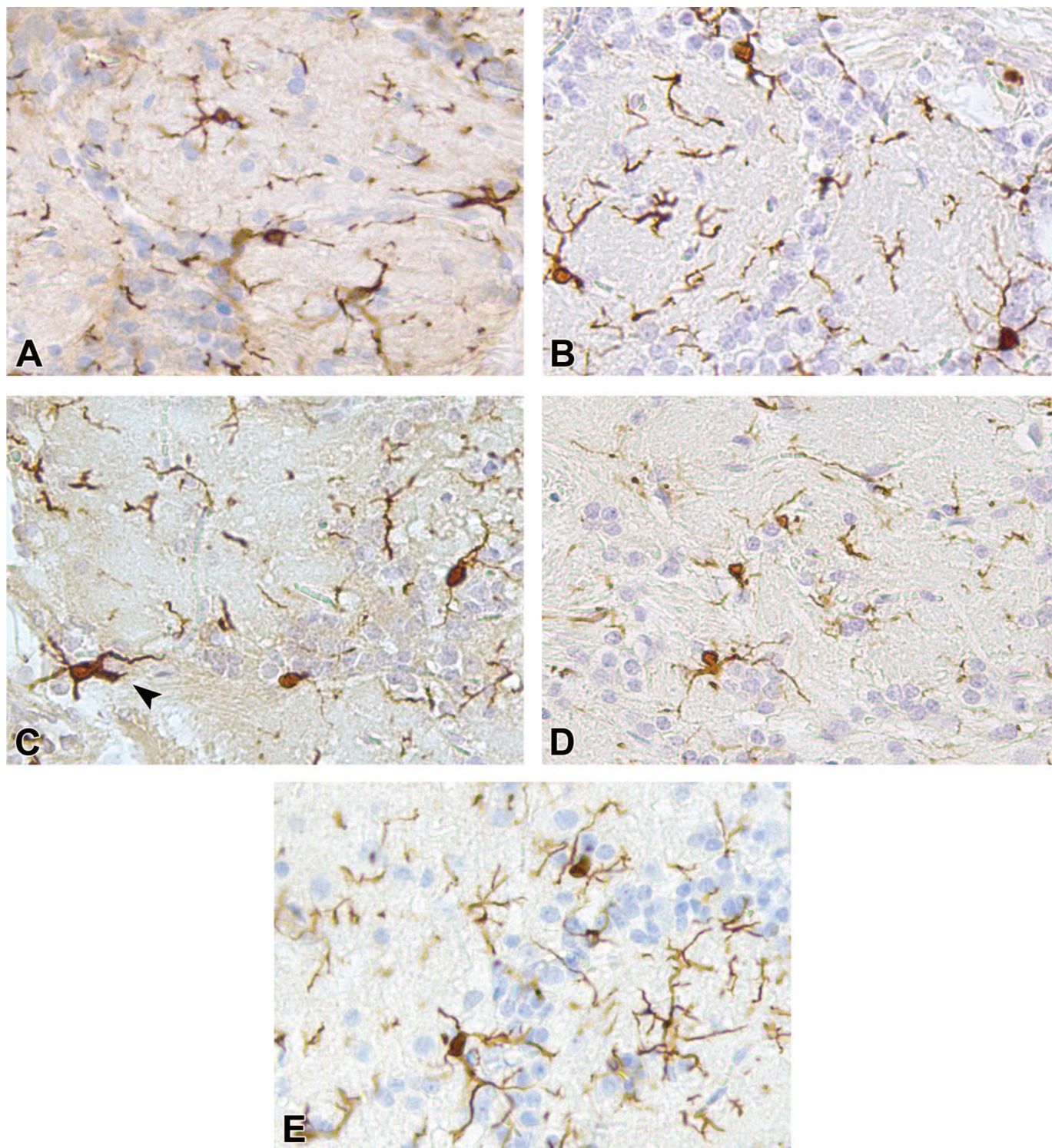


Figure 8. Representative brightfield microscopy images of the glomerular layer of the olfactory bulb tissue sections, at original objective 20X, with anti-ionized calcium-binding adapter molecule 1 immunohistochemical stain to visualize microglial cells (sham control [A], day 0 post-exposure [B], day 1 post-exposure [C], day 7 post-exposure [D], day 21 post-exposure [E]). Arrowhead points to activated microglia.

inhaled AgNPs of similar diameter to ours were detected in the OB with peak concentration immediately after a 6-hour inhalation exposure period and again at D7 post-exposure.⁶² Patchin et al.²⁶ found significant microglial activation in the OB

immediately after exposure to similarly sized inhaled AgNPs and at D1 and D7 post-exposure. These temporal profiles are similar to our finding of microglial activation in the OB on D1 and D7 post-exposure. The first peak in Ag deposition and early

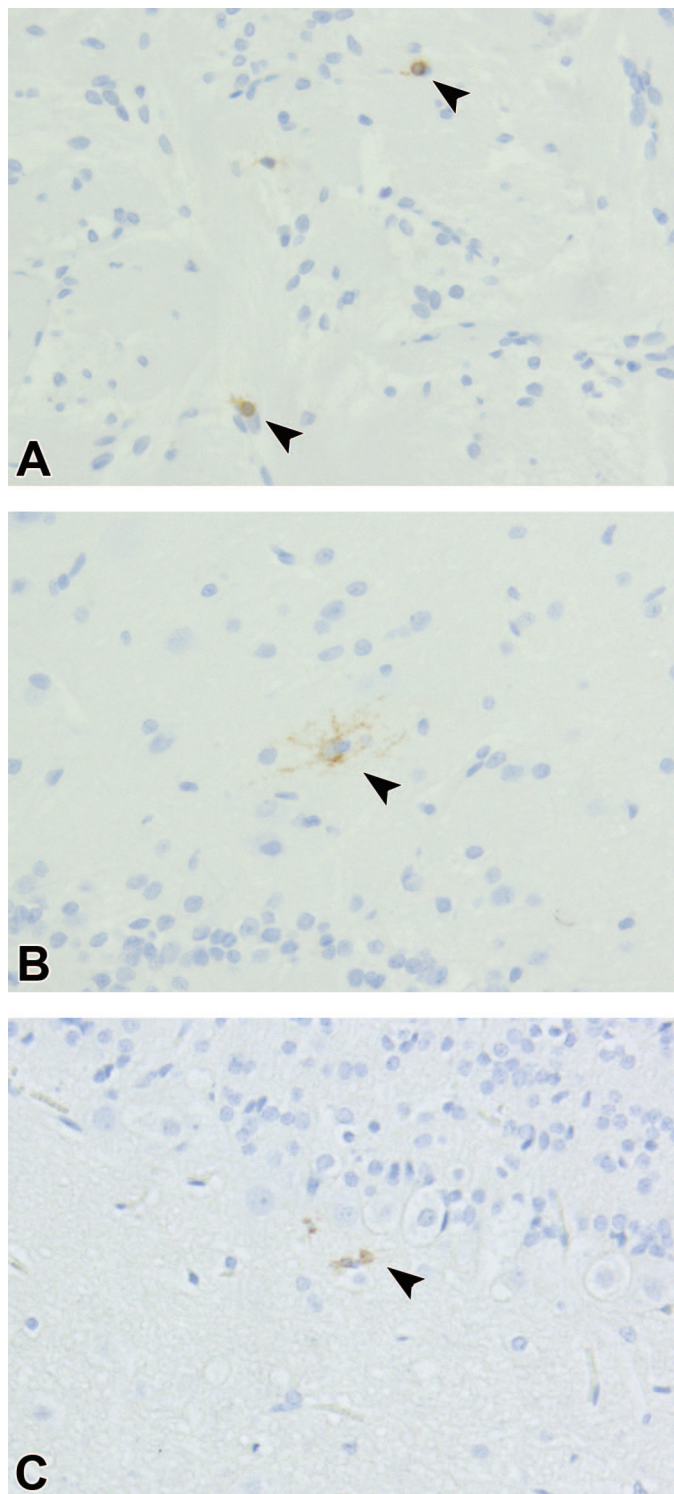


Figure 9. Representative brightfield microscopy images of olfactory bulb tissue sections, at original objective 20X, with anti-heme oxygenase-I immunohistochemical stain showing immunostaining on post-exposure day 0 (A), day 1 (B), and day 7 (C). Arrowheads point to cells with heme oxygenase-I staining, a marker for oxidative stress.

microglial activation may represent translocation of NPs via the intra-neuronal olfactory pathway as well as systemic absorption

of NPs via the gastrointestinal tract and the hepatic portal circulation. Recordati et al.⁶³ showed that ingestion of AgNPs was correlated with structural alteration of the blood-brain barrier, which may facilitate AgNPs entry to the CNS. The second peak in Ag deposition and delayed microglial activation may represent NPs entering the systemic circulation and lymphatics following delayed clearance from the nasal cavity and lungs.^{26,62,64}

Recruitment of additional microglia to the OB is another marker of pro-inflammatory response that has been reported following exposure to NP.⁶⁵ We did not find a significant increase in the number of microglia in the OB in animals exposed to Ag-SiO₂ NPs compared with controls at any post-exposure time point (Figure 6). This suggested a non-inflammatory response to inhaled Ag-SiO₂ NPs. This is further supported by a mild oxidative stress response indicated by sparse HO-1 immunostaining in the OB. These findings, taken altogether, suggested an insignificant inflammatory response in the OB to inhaled Ag-SiO₂ NPs. The exposure time to NPs in this study (single, 6-hour inhalation) may not be sufficiently long to elicit microglial recruitment to the OB. Wang et al.⁶⁵ found microglial recruitment to the OB following every other day instillation of NPs over a period of 40 days. Second, the silicate core of the Ag-SiO₂ NPs conferred stability to the structure and may have caused the AgNPs to oxidize more slowly to Ag⁺, thus minimizing injury to cells in the OB.¹³ Aggregation of Ag-SiO₂ NPs during aerosolization, as shown by the aerosol diameter measured by the cascade impactor, may have also reduced NPs deposition onto the nasal epithelium, which in turn diminished cellular uptake efficiency and cytotoxic effects on microglial cells in the OB. This presumption is supported by previous studies that demonstrated decreased cellular uptake rates of large-sized NPs compared with smaller-sized NPs of the same composition.^{66,67} Further studies with sub-acute and chronic exposure durations are needed to fully evaluate the extent of Ag-SiO₂ NP-induced inflammation in the OB.

Differential activation of microglia was noted among the histologically distinct layers of the OB. This differential activation of microglia may potentially be due to NPs failing to penetrate deeper into the OB. However, previous studies found metal NPs along with associated microglial activation and histologic brain remodeling in the OB and more distant brain regions such as the hippocampus, striatum, and lateral ventricle following inhalation and intranasal instillation of metal NPs.^{37,60,65,68,69} These findings suggested that the acute inhalation exposure duration may have precluded delivery of a dose of metal NPs equivalent to chronic inhalation or intranasal instillation leading to less NPs deposition onto the olfactory epithelium, less NPs translocation to the deeper layers of the OB, and less microglial activation than expected.

The major limitation of this study is that the activation of microglia in the OB showed implied rather than actual translocation of AgNPs from the nasal cavity to the OB. We were unable to visualize or quantify silver in the nasal cavity, the olfactory nerves, or in the OB using autometallography or ICP-MS. Other studies used these methods to demonstrate presence of silver in these tissues, but we were unable to

replicate this result.^{25,26} One reason for this may be due to the interaction between EDTA used for decalcification of the nasal cavity and the silver enhancement solution used in autometallography. Autometallography utilizes gold to initiate the reduction of ionic silver to metallic silver.⁷⁰ EDTA is commonly used as a metal chelator and is capable of chelating gold.⁷¹⁻⁷³ These reagents may have cross-reacted to cause gold to precipitate out of the solution rather than aid in ionic silver reduction for visualization. Another explanation may be that the amount of AgNPs deposited was insufficient for direct silver visualization due to the low dose of exposure or due to NP agglomeration precluding efficient NP deposition onto the nasal epithelium as discussed above. Further studies are needed to investigate the in vivo translocation of inhaled Ag-SiO₂ NPs to the CNS.

Another limitation of the study was that we did not differentiate between activated microglia from CNS-associated macrophages, which have a similar amoeboid morphology. Microglia and CNS-associated macrophages are resident immune cells of the CNS but reside in different niches. Microglia reside in the brain parenchyma, whereas CNS-associated macrophages are non-parenchymal and reside in peripheral regions such as the perivascular space, choroid plexus, and meninges.⁷⁴ Iba1, the immunohistochemical marker chosen for this study, is widely used to highlight microglia, but it can also bind to macrophages.^{75,76} Our OB sections likely had perivascular macrophages but not choroidal or meningeal macrophages, as these structures were not attached to the OB sections used for analysis. Without differentially staining for these cells, we may have classified some perivascular macrophages as activated microglia. However, perivascular macrophages are normal immune cells of the CNS and are present in both sham control as well as exposure groups. Moreover, perivascular macrophages may also proliferate in response to CNS injury.⁷⁷ Therefore, by comparing the ratio of activated to resting microglia rather than total count of activated microglia, we were still able to utilize morphometric analysis of microglia to indirectly assess the inflammatory response in the OB in response to inhaled Ag-SiO₂ NPs. Further studies are needed to assess the activation pattern of microglia and CNS-associated macrophages following inhalation of Ag-SiO₂ NPs, as their activation pattern may have implications on the route NPs may take to enter the CNS. Activation of microglia but not CNS-associated macrophages may suggest a primarily intra-neuronal transport of NPs to the CNS to induce an inflammatory response in parenchymal immune cells. On the contrary, activation of CNS-associated macrophages but not microglia may suggest a primarily extra-neuronal or systemic transport of NPs.

Conclusion

Acute inhalation of Ag-SiO₂ NPs elicited transient and differential microglial activation without significant microglial recruitment to the OB. The delayed and differential pattern of microglial activation in the OB implied that inhaled Ag-SiO₂ NPs may have translocated to the CNS via intra-neuronal

pathway. The absence of significant microglial recruitment and mild oxidative stress in the OB was indicative of an insignificant inflammatory response in the OB that might reflect the short duration of the acute inhalation exposure, the chemical stability of the Ag-SiO₂ NPs conferred by the silicate core, or moderate Ag-SiO₂ NPs agglomeration during aerosolization that interfered with NPs deposition onto the nasal epithelium, which in turn diminish the number of NPs available to reach distant organs to induce cytotoxic effects.

Acknowledgments

The authors thank Dale Uyeminami, Neha Singh, and Ching-Wen Wu for technical assistance and Rona Silva for proofreading.

Declaration of Conflicting Interests


The author(s) declared no potential conflicts of interest with respect to the research, authorship, and/or publication of this article.

Funding

The author(s) disclosed receipt of the following financial support for the research, authorship, and/or publication of this article: Grant support for this study were from the National Institute of Environmental Health Sciences U01 ES027288, P30 ES023513, P51 OD011107. The silver nanomaterials used in this study were procured, characterized, and provided to investigators by the National Institute of Environmental Health Sciences (NIEHS) Centers for Nanotechnology Health Implications Research (NCNHIR) Consortium. Financial support was provided by the Students Training in Advanced Research (STAR) Program through a University of California-Davis School of Veterinary Medicine Endowment Fund.

ORCID iDs

Huong Huynh  <https://orcid.org/0000-0002-2277-1821>

Kent E. Pinkerton  <https://orcid.org/0000-0001-6868-7572>

References

- Shao Y, Wu C, Wu T, et al. Green synthesis of sodium alginate-silver nanoparticles and their antibacterial activity. *Int J Biol Macromol*. 2018;111:1281-1292. doi:10.1016/j.ijbiomac.2018.01.012.
- Kumar R, Howdle S, Münstedt H. Polyamide/silver antimicrobials: effect of filler types on the silver ion release. *J Biomed Mater Res Part B: Applied Biomaterials*. 2005;75B(2):311-319. doi:10.1002/jbm.b.30306.
- Burdu el AC, Gherasim O, Grumezescu AM, Mogoantă L, Ficai A, Andronescu E. Biomedical applications of silver nanoparticles: an up-to-date overview. *Nanomaterials (Basel)*. 2018;8(9):681. doi:10.3390/nano8090681.
- Lem KW, Choudhury AA, Lakhani A, et al. Use of nanosilver in consumer products. *NANOTEC*. 2012;6(1):60-72. doi:10.2174/187221012798109318.
- Larese FF, D'Agostin F, Crosera M, et al. Human skin penetration of silver nanoparticles through intact and damaged skin. *Toxicology*. 2009;255(1):33-37. doi:10.1016/j.tox.2008.09.025.
- George R, Merten S, Wang TT, Kennedy P, Maitz P. In vivo analysis of dermal and systemic absorption of silver nanoparticles through healthy human skin. *Austral J Dermatol*. 2014;55(3):185-190. doi:10.1111/ajd.12101.
- Kim S, Gates BL, Chang M, et al. Transcorneal delivery of topically applied silver nanoparticles does not delay epithelial wound healing. *Nanoimpact*. 2021;24:100352. doi:10.1016/j.impact.2021.100352.

8. Johnston HJ, Hutchison G, Christensen FM, Peters S, Hankin S, Stone V. A review of the in vivo and in vitro toxicity of silver and gold particulates: particle attributes and biological mechanisms responsible for the observed toxicity. *Crit Rev Toxicol*. 2010;40(4):328-346. doi:10.3109/10408440903453074.
9. Bourquin J, Milosevic A, Hauser D, et al. Biodistribution, clearance, and long-term fate of clinically relevant nanomaterials. *Adv Mater*. 2018;30(19):1704307. doi:10.1002/adma.201704307.
10. Suresh AK, Pelletier DA, Wang W, Morrell-Falvey JL, Gu B, Doktycz MJ. Cytotoxicity induced by engineered silver nanocrystallites is dependent on surface coatings and cell types. *Langmuir*. 2012;28(5):2727-2735. doi:10.1021/la2042058.
11. Jo DH, Kim JH, Lee TG, Kim JH. Size, surface charge, and shape determine therapeutic effects of nanoparticles on brain and retinal diseases. *Nanomed: Nanotechnol*. 2015;11(7):1603-1611. doi:10.1016/j.nano.2015.04.015.
12. Riaz Ahmed KB, Nagy AM, Brown RP, Zhang Q, Malghan SG, Goering PL. Silver nanoparticles: significance of physicochemical properties and assay interference on the interpretation of in vitro cytotoxicity studies. *Toxicol in Vitro*. 2017;38:179-192. doi:10.1016/j.tiv.2016.10.012.
13. Jiang ZJ, Liu CY, Sun LW. Catalytic properties of silver nanoparticles supported on silica spheres. *J Phys Chem B*. 2005;109(5):1730-1735. doi:10.1021/jp046032g.
14. Chu CY, Peng FC, Chiu YF, et al. Nanohybrids of silver particles immobilized on silicate platelet for infected wound healing. *PLOS ONE*. 2012;7(6):e38360. doi:10.1371/journal.pone.0038360.
15. Egger S, Lehmann RP, Height MJ, Loessner MJ, Schuppler M. Antimicrobial properties of a novel silver-silica nanocomposite material. *Appl Environ Microbiol*. 2009;75:2973-2976. doi:10.1128/AEM.01658-08.
16. Mannu R, Karthikeyan V, Veerappa MM, et al. Facile use of silver nanoparticles-loaded alumina/silica in nanofluid formulations for enhanced catalytic performance toward 4-nitrophenol reduction. *Int J Environ Res Public Health*. 2021;18(6):2994. doi:10.3390/ijerph18062994.
17. Neves J, das Arzi RS, Sosnik A. Molecular and cellular cues governing nanomaterial-mucosae interactions: from nanomedicine to nanotoxicology. *Chem Soc Rev*. 2020;49:5058-5100. doi:10.1039/C8CS00948A.
18. Illum L. Transport of drugs from the nasal cavity to the central nervous system. *Eur J Pharm Sci*. 2000;11(1):1-18. doi:10.1016/S0928-0987(00)00087-7.
19. Crowe TP, Greenlee MHW, Kanthasamy AG, Hsu WH. Mechanism of intranasal drug delivery directly to the brain. *Life Sci*. 2018;195:44-52. doi:10.1016/j.lfs.2017.12.025.
20. Selvaraj K, Gowthamarajan K, Karri VVSR. Nose to brain transport pathways an overview: potential of nanostructured lipid carriers in nose to brain targeting. *Artif Cell Nanomed B*. 2018;46:2088-2095. doi:10.1080/21691401.2017.1420073.
21. van Riel D, Verdijk R, Kuiken T. The olfactory nerve: a shortcut for influenza and other viral diseases into the central nervous system. *J Pathol*. 2015;235(2):277-287. doi:10.1002/path.4461.
22. Meinhardt J, Radke J, Dittmayer C, et al. Olfactory transmucosal SARS-CoV-2 invasion as a port of central nervous system entry in individuals with COVID-19. *Nat Neurosci*. 2021;24(2):168-175. doi:10.1038/s41593-020-00758-5.
23. Ji JH, Jung JH, Kim SS, et al. Twenty-eight-day inhalation toxicity study of silver nanoparticles in Sprague-Dawley rats. *Inhal Toxicol*. 2007;19(10):857-871. doi:10.1080/08958370701432108.
24. Sung JH, Ji JH, Park JD, et al. Subchronic inhalation toxicity of silver nanoparticles. *Toxicol Sci*. 2009;108(2):452-461. doi:10.1093/toxsci/kfn246.
25. Genter MB, Newman NC, Shertzer HG, Ali SF, Bolon B. Distribution and systemic effects of intranasally administered 25 nm silver nanoparticles in adult mice. *Toxicol Pathol*. 2012;40(7):1004-1013. doi:10.1177/0192623312444470.
26. Patchin ES, Anderson DS, Silva RM, et al. Size-dependent deposition, translocation, and microglial activation of inhaled silver nanoparticles in the rodent nose and brain. *Environ Health Perspect*. 2016;124(12):1870-1875. doi:10.1289/EHP234.
27. Hopkins LE, Patchin ES, Chiu PL, Brandenberger C, Smiley-Jewell S, Pinkerton KE. Nose-to-brain transport of aerosolized quantum dots following acute exposure. *Nanotoxicology*. 2014;8(8):885-893. doi:10.3109/17435390.2013.842267.
28. Elder A, Gelein R, Silva V, et al. Translocation of inhaled ultrafine manganese oxide particles to the central nervous system. *Environ Health Perspect*. 2006;114(8):1172-1178. doi:10.1289/ehp.9030.
29. de Castro F. Wiring olfaction: the cellular and molecular mechanisms that guide the development of synaptic connections from the nose to the cortex. *Front Neurosci*. 2009;3:52. doi:10.3389/neuro.22.004.2009.
30. Kosada T, Kosada K. Olfactory bulb anatomy. In: Squire LR, ed. *Encyclopedia of Neuroscience*. 1st ed. Cambridge, MA: Academic Press; 2009:59-69.
31. Wake H, Moorhouse AJ, Jinno S, Kohsaka S, Nabekura J. Resting microglia directly monitor the functional state of synapses in vivo and determine the fate of ischemic terminals. *J Neurosci*. 2009;29(13):3974-3980. doi:10.1523/JNEUROSCI.4363-08.2009.
32. Tremblay MÈ, Stevens B, Sierra A, Wake H, Bessis A, Nimmerjahn A. The role of microglia in the healthy brain. *J Neurosci*. 2011;31(45):16064-16069. doi:10.1523/JNEUROSCI.4158-11.2011.
33. Schafer DP, Lehrman EK, Kautzman AG, et al. Microglia sculpt postnatal neural circuits in an activity and complement-dependent manner. *Neuron*. 2012;74(4):691-705. doi:10.1016/j.neuron.2012.03.026.
34. Squarzone P, Oller G, Hoeffel G, et al. Microglia modulate wiring of the embryonic forebrain. *Cell Reports*. 2014;8(5):1271-1279. doi:10.1016/j.celrep.2014.07.042.
35. Tin-Tin-Win-Shwe, Yamamoto S, Ahmed S, Kakeyama M, Kobayashi T, Fujimaki H. Brain cytokine and chemokine mRNA expression in mice induced by intranasal instillation with ultrafine carbon black. *Toxicology Letters*. 2006;163(2):153-160. doi:10.1016/j.toxlet.2005.10.006.
36. Hutter E, Boridy S, Labrecque S, et al. Microglial response to gold nanoparticles. *ACS Nano*. 2010;4(5):2595-2606. doi:10.1021/nn901869f.
37. Ze Y, Sheng L, Zhao X, et al. TiO₂ nanoparticles induced hippocampal neuroinflammation in mice. *PLOS ONE*. 2014;9(3):e92230. doi:10.1371/journal.pone.0092230.
38. Foldbjerg R, Olesen P, Hougaard M, Dang DA, Hoffmann HJ, Autrup H. PVP-coated silver nanoparticles and silver ions induce reactive oxygen species, apoptosis and necrosis in THP-1 monocytes. *Toxicology Letters*. 2009;190(2):156-162. doi:10.1016/j.toxlet.2009.07.009.
39. Wang X, Ji Z, Chang CH, et al. Use of coated silver nanoparticles to understand the relationship of particle dissolution and bioavailability to cell and lung toxicological potential. *Small*. 2014;10(2):385-398. doi:10.1002/smll.201301597.
40. Wang L, Zhang T, Li P, et al. Use of synchrotron radiation-analytical techniques to reveal chemical origin of silver-nanoparticle cytotoxicity. *ACS Nano*. 2015;9(6):6532-6547. doi:10.1021/acsnano.5b02483.
41. Beltran-Huacac J, Zhang Z, Pyrgiotakis G, DeLoid G, Vaze N, Demokritou P. Development of reference metal and metal oxide engineered nanomaterials for nanotoxicology research using high throughput and precision flame spray synthesis approaches. *Nanoimpact*. 2018;10:26-37. doi:10.1016/j.impact.2017.11.007.
42. Zhang T, Gaffrey MJ, Thomas DG, et al. A proteome-wide assessment of the oxidative stress paradigm for metal and metal-oxide nanomaterials in human macrophages. *Nanoimpact*. 2020;17:100194. doi:10.1016/j.impact.2019.100194.
43. Raabe OG, Bennick JE, Light ME, Hobbs CH, Thomas RL, Tillery MI. An improved apparatus for acute inhalation exposure of rodents to radioactive aerosols. *Toxicol Appl Pharmacol*. 1973;26(2):264-273. doi:10.1016/0041-008x(73)90261-5.
44. Anderson DS, Patchin ES, Silva RM, et al. Influence of particle size on persistence and clearance of aerosolized silver nanoparticles in the rat lung. *Toxicol Sci*. 2015;144(2):366-381. doi:10.1093/toxsci/kfv005.
45. Ruehl-Fehlert C, Kittel B, Morawietz G, et al. Revised guides for organ sampling and trimming in rats and mice—part 1. *Exp Toxicol Pathol*. 2003;55(2-3):91-106.

46. Hanisch UK, Kettenmann H. Microglia: active sensor and versatile effector cells in the normal and pathologic brain. *Nat Neurosci.* 2007;10(11):1387-1394. doi:10.1038/nn1997.
47. Olah M, Biber K, Vinet JWGM, Boddeke H. Microglia phenotypic diversity. *CNSNDT.* 2011;10(1):108-118. doi:10.2174/187152711794488575.
48. Davalos D, Grutzendler J, Yang G, et al. ATP mediates rapid microglial response to local brain injury in vivo. *Nat Neurosci.* 2005;8(6):752-758. doi:10.1038/nn1472.
49. Nimmerjahn A, Kirchhoff F, Helmchen F. Resting microglial cells are highly dynamic surveillants of brain parenchyma in vivo. *Science.* 2005;308(5726):1314-1318. doi:10.1126/science.1110647.
50. Cherry JD, Olschowka JA, O'Banion MK. Neuroinflammation and M2 microglia: the good, the bad, and the inflamed. *J Neuroinflammation.* 2014;11(1):98. doi:10.1186/1742-2094-11-98.
51. Stence N, Waite M, Dailey ME. Dynamics of microglial activation: a confocal time-lapse analysis in hippocampal slices. *Glia.* 2001;33(3):256-266. doi:10.1002/1098-1136(200103)33:3<256::AID-GLIA1024>3.0.CO;2-J.
52. Ghasemi A, Zahediasl S. Normality tests for statistical analysis: a guide for non-statisticians. *Int J Endocrinol Metab.* 2012;10(2):486-489. doi:10.5812/ijem.3505.
53. Yan F, Robert M, Li Y. Statistical methods and common problems in medical or biomedical science research. *Int J Physiol Pathophysiol Pharmacol.* 2017;9(5):157-163.
54. Garcia GJM, Kimbell JS. Deposition of inhaled nanoparticles in the rat nasal passages: dose to the olfactory region. *Inhalation Toxicology.* 2009;21(14):1165-1175. doi:10.3109/08958370902882713.
55. Occupational Safety and Health Administration. *Silver, metal, and soluble compounds (As Ag+).* 1988. Accessed March 2, 2022. <https://www.osha.gov/chemicaldata/519>.
56. Lee JH, Ahn K, Kim SM, Jeon KS, Lee JS, Yu IJ. Continuous 3-day exposure assessment of workplace manufacturing silver nanoparticles. *J Nanopart Res.* 2012;14(9):1134. doi:10.1007/s11051-012-1134-8.
57. Luther EM, Petters C, Bulcke F, et al. Endocytotic uptake of iron oxide nanoparticles by cultured brain microglial cells. *Acta Biomaterialia.* 2013;9(9):8454-8465. doi:10.1016/j.actbio.2013.05.022.
58. Ye D, Raghnaill MN, Bramini M, et al. Nanoparticle accumulation and transcytosis in brain endothelial cell layers. *Nanoscale.* 2013;5(22):11153-11165. doi:10.1039/C3NR02905K.
59. Wang J, Liu Y, Jiao F, et al. Time-dependent translocation and potential impairment on central nervous system by intranasally instilled TiO₂ nanoparticles. *Toxicology.* 2008;254(1):82-90. doi:10.1016/j.tox.2008.09.014.
60. Liu Y, Gao Y, Liu Y, Li B, Chen C, Wu G. Oxidative stress and acute changes in murine brain tissues after nasal instillation of copper particles with different sizes. *J Nanosci Nanotechnol.* 2014;14(6):4534-4540. doi:10.1166/jnn.2014.8290.
61. Duffy CM, Ahmed S, Yuan C, Mavanji V, Nixon JP, Butterick T. Microglia as a surrogate biosensor to determine nanoparticle neurotoxicity. *J Vis Exp.* 2016(116):54662. doi:10.3791/54662.
62. Andriamasinoro SN, Dieme D, Marie-Desvergne C, et al. Kinetic time courses of inhaled silver nanoparticles in rats. *Arch Toxicol.* 2022;96(2):487-498. doi:10.1007/s00204-021-03191-0.
63. Recordati C, De Maglie M, Cella C, et al. Repeated oral administration of low doses of silver in mice: tissue distribution and effects on central nervous system. *Part Fibre Toxicol.* 2021;18(1):23. doi:10.1186/s12989-021-00418-x.
64. Kim JK, Kim HP, Park JD, et al. Lung retention and pharmacokinetics of silver and gold nanoparticles in rats following subacute inhalation co-exposure. *Part Fibre Toxicol.* 2021;18:5. doi:10.1186/s12989-021-00397-z.
65. Wang Y, Wang B, Zhu MT, et al. Microglial activation, recruitment and phagocytosis as linked phenomena in ferric oxide nanoparticle exposure. *Toxicology Letters.* 2011;205(1):26-37. doi:10.1016/j.toxlet.2011.05.001.
66. Zhu J, Liao L, Zhu L, et al. Size-dependent cellular uptake efficiency, mechanism, and cytotoxicity of silica nanoparticles toward HeLa cells. *Talanta.* 2013;107:408-415. doi:10.1016/j.talanta.2013.01.037.
67. Wu M, Guo H, Liu L, Liu Y, Xie L. Size-dependent cellular uptake and localization profiles of silver nanoparticles. *Int J Nanomedicine.* 2019;14:4247-4259. doi:10.2147/IJN.S201107.
68. Davenport LL, Hsieh H, Eppert BL, et al. Systemic and behavioral effects of intranasal administration of silver nanoparticles. *Neurotoxicol Teratol.* 2015;51:68-76. doi:10.1016/j.ntt.2015.08.006.
69. Lebedová J, Nováková Z, Večeřa Z, et al. Impact of acute and subchronic inhalation exposure to PbO nanoparticles on mice. *Nanotoxicology.* 2018;12(4):290-304. doi:10.1080/17435390.2018.1438679.
70. Danscher G. Autometallography: a new technique for light and electron microscopic visualization of metals in biological tissues (gold, silver, metal sulphides and metal selenides). *Histochemistry.* 1984;81(4):331-335. doi:10.1007/BF00514327.
71. Oviedo C, Rodríguez J. EDTA: the chelating agent under environmental scrutiny. *Quím Nova.* 2003;26:901-905. doi:10.1590/S0100-40422003000600020.
72. Flora SJS, Pachauri V. Chelation in metal intoxication. *Int J Environ Res Public Health.* 2010;7(7):2745-2788. doi:10.3390/ijerph7072745.
73. Sreepasad TS, Pradeep T. Reversible assembly and disassembly of gold nanorods induced by EDTA and its application in SERS tuning. *Langmuir.* 2011;27(7):3381-3390. doi:10.1021/la104828e.
74. Herz J, Filiano AJ, Smith A, Yorgev N, Kipnis J. Myeloid cells and their relationship with the central nervous system. *Immunity.* 2017;46(6):943-956. doi:10.1016/j.immuni.2017.06.007.
75. Sasaki Y, Ohsawa K, Kanazawa H, Kohsaka S, Imai Y. Iba1 is an actin-cross-linking protein in macrophages/microglia. *Biochem Biophys Res Commun.* 2001;286(2):292-297. doi:10.1006/bbrc.2001.5388.
76. Jurga AM, Paleczna M, Kuter KZ. Overview of general and discriminating markers of differential microglia phenotypes. *Front Cell Neurosci* 2020;14:198. Accessed April 22, 2022. <https://www.frontiersin.org/article/10.3389/fncel.2020.00198>.
77. Greenhalgh AD, Zarruk JG, Healy LM, et al. Peripherally derived macrophages modulate microglial function to reduce inflammation after CNS injury. *PLOS Biol.* 2018;16(10):e2005264. doi:10.1371/journal.pbio.2005264.